Available online at www.sciencedirect.com
SCIENCE DIRECT®
Journal of Magnetic Resonance 167 (2004) 87–96
JMR Journal of Magnetic Resonance
www.elsevier.com/locate/jmr

Implementing solenoid microcoils for wide-line solid-state NMR

K. Yamauchi, J.W.G. Janssen, and A.P.M. Kentgens*

Department of Physical Chemistry/Solid-State NMR, NSRIM Center, University of Nijmegen, Toernooiveld 1, 6525 ED Nijmegen, The Netherlands

Received 18 August 2003; revised 2 December 2003

Abstract

Solid-state nuclear magnetic resonance (NMR) probeheads using solenoid microcoils with an inner diameter of 300–400 μm are developed for the study of mass-limited solid samples. Some attention is paid to the mechanical ruggedness of the probes allowing sample changing. The performance, in terms of sensitivity and RF-characteristics, of these probeheads is studied for ^{1}H, ^{31}P, and ^{27}Al in different model compounds in view of the feasibility of specific applications. The results show that the sensitivity is high enough to detect approximately 10^{14} spins/$\sqrt{Hz}$ with a signal-to-noise ratio of 1 in a single scan. A specific advantage of microcoils for solid-state NMR applications is that they can generate extremely high RF-fields if implemented in appropriate circuits. Using RF-powers in the hundreds of Watts range, RF-fields well in excess of 1 MHz can be made. This allows the excitation of spectra of nuclei whose resonance lines are dispersed of several megahertz. This is particularly useful for quadrupolar nuclei experiencing large quadrupolar interactions as is demonstrated for ^{27}Al in single crystal and powdered minerals.

Keywords: Microcoil; Limit of detection; Solid-state NMR; High RF-field; Quadrupolar nuclei

1. Introduction

Nuclear magnetic resonance (NMR) spectroscopy has developed into one of the most powerful analysis techniques in (bio)chemistry, materials science, geology, medicine, etc. in both solution and solid-state. A major disadvantage of NMR, compared to other analytical methods is its relative insensitivity, as a result of which only bulk properties of materials can be obtained. In case of non-lossy samples, the sensitivity of the RF-coil is one of the major factors determining the experimental sensitivity. Hoult and Richards [1] introduced the concept that the voltage induced in a coil by the precessing magnetization of a sample is proportional to magnetic field per unit current that can be generated in the coil by passing a current through it. Straightforward calculations show that there is a reciprocal relationship between the coil sensitivity and the diameter of a solenoid at a fixed length to diameter ratio. These considerations furthermore show that if sufficient amounts of sample are available, and bulk properties of the material have to be determined, it is advantageous to work with large samples and an appropriate coil volume. If the amount of sample is limited, however, sensitivity can be gained by decreasing the coil size in order to keep the filling factor as large as possible. It is for this reason that a lively research has sprung up in high-resolution NMR to be able to study mass or volume-limited samples as is, e.g., encountered when combining liquid chromatography and NMR [2–7]. Similarly in MRI there is an urge to image ever-smaller structures, which can only be achieved by using smaller and smaller coils [8–11].

In solid-state NMR there are also clear objectives underpinning the necessity to implement microcoils in specific cases. As in the case of liquids, the possibility to analyze very small amounts of sample is imperative if the availability of such sample is limited, e.g., due to complicated sample preparation pathways. In solids we distinguish two cases, one is where the absolute amount of sample is restricted, e.g., for isotopically enriched biological samples, and the second case is where there are no crystals of sufficient size available in cases where a single-crystal study is called for. The latter situation is encountered for zeolites. Although zeolite samples are readily available it is in general not possible to get single

* Corresponding author. Fax: +31-24-3652112.
E-mail address: arno@solidmr.kun.nl (A.P.M. Kentgens).

1090-7807/$ - see front matter © 2003 Elsevier Inc. All rights reserved.
doi:10.1016/j.jmr.2003.12.003

crystals of several tens of micrometer for Al-containing samples. However, a single-crystal study of such a sample would directly reveal the different crystallographic sites, their occupancy, and the associated quadrupolar parameters.

Because of the inherently small sample volume in the microcoil, the homogeneity of the external field is less stringent. Therefore their implementation is of interest for performing NMR experiments in high-field Bitter magnets [12–14] or in the inherently inhomogeneous fields of devices using permanent magnets such as the NMR mouse [15]. A final advantage of the microcoils, related to their sensitivity through the reciprocity theorem, is the capability to generate very high RF-fields per unit current. Therefore if the microcoil probehead is designed to handle the same power as a regular NMR probe, much higher RF-fields can be generated. Alternatively, RF-fields comparable to those employed in normal NMR probes can be generated with very low power so that one does not need specific high-power amplifiers. As the Q of the microcoils is comparatively low (10–40) receiver dead times can also be very short which is advantageous for the direct detection of broad lines.

In view of the considerations described above we have developed and tested a number of microcoil probeheads using solenoid coils with an inner diameter of 300 and 400 μm. The different designs were optimized for proton observation, X-nuclei detection and broadband operation, respectively. The setups were optimized for RF-performance and mechanical stability allowing operation as a regular NMR probehead. This manuscript describes the designs and their performance in terms of sensitivity, resolution, and RF-field strength. The latter is exploited for the observation of ^{27}Al in single crystalline and powdered minerals.

2. Probehead design

The design of microcoils for high-resolution NMR and MR imaging purposes has been reviewed by Webb [4] and Minard and Wind [16,17]. Based on the work by Hoult and Richards [1] and Hoult [18] the S/N in an NMR experiment is defined as the peak signal divided by the root mean square noise:

$$\frac{S}{N} = \frac{k_0\left(\frac{B_1}{i}\right) V_S N \gamma \hbar^2 I(I+1) \frac{\omega_0^2}{k_B T 3\sqrt{2}}}{F\sqrt{4 k_B T R_{\text{noise}} \Delta f}}, \quad (1)$$

where k_0 is a scaling factor accounting for the RF-inhomogeneity of the coil, B_1/i the magnetic field induced in the RF-coil per unit current, V_S the sample volume, N the number spins of interest per unit volume, γ the gyromagnetic ratio, I the spin quantum number, ω_0 the nuclear Larmor precession frequency, T the temperature, and h and k_B are Planck's and Boltzmann's constant, respectively. The denominator describes the noise using the noise factor of the spectrometer (F), conductive losses of the coil, circuit and sample (R_{noise}), and the spectral bandwidth (Δf). For an evenly spaced, closely wound, solenoid coil, allowing the coil to be approximated as a sum of current loops, the on-axis B_1-field can be calculated using the Biot–Savart law:

$$\frac{B_1}{i} = \mu_0 n \left(\frac{\frac{x}{l} + \frac{1}{2}}{\sqrt{4r^2 + (2x+l)^2}} - \frac{\frac{x}{l} - \frac{1}{2}}{\sqrt{4r^2 + (2x-l)^2}} \right), \quad (2)$$

where the origin of x is defined at the center of the coil. μ_0 is the permeability of free space, n the number of turns in the coil, and r and l are the radius and length of the coil. At the center of the coil ($x = 0$) this reduces to

$$\frac{B_1}{i} = \frac{\mu_0 n}{2r} \frac{1}{\sqrt{1 + (l/2r)^2}} \quad (3)$$

showing that the coil sensitivity increases with the inverse of the diameter for coils with a fixed form factor $l/2r$, which is the rationale for using microcoils to get NMR spectra from mass/volume-limited samples.

As can be seen from Eq. (1) the S/N achievable in a microcoil critically depends on the resistance of the coil. This resistance is determined by the size and geometry of the coil and the frequency of operation. A further important factor in the design is to minimize losses from the coil leads and the capacitors used to tune the circuit. We have come up with a parallel capacitor and coil circuit in which the coil is mechanically integrated in a custom made capacitor as displayed in Fig. 1. This design not only minimizes the use of parasitic leads, it also gives mechanical stability to the coil so that sample changing can be readily achieved without damage to the circuit. The coils are mounted on a micro-machined cylindrical holder with an open inner diameter of 200–300 μm for sample insertion. The outside of the holder is threaded so that an evenly spaced coil can be wound onto it. The coil is then secured onto the cylindrical holder using a KEL-F sleeve. This rigid coil construction is tightly fitted into a central hole in the capacitor

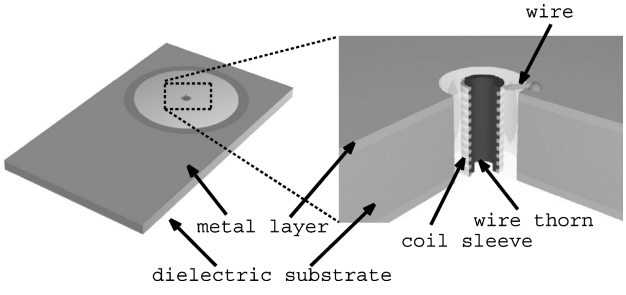

Fig. 1. Illustration of the parallel resonance circuit with sample coil and capacitor (left) and a detailed view of the coil construction (right).

and the coil leads are either glued (with silver paint) or soldered to the capacitor plates. Two similarly designed single-channel probeheads were built for the observation of protons at 400 MHz, and X-nuclei around ~160 MHz, respectively.

The proton probe was fitted with a coil consisting of 11 windings wound from round copper wire ($\varnothing = 50\,\mu m$) onto a vespel holder with a threaded outer diameter of 400 μm and an inner opening of 300 μm. The spacing of the leads is 90 μm giving us a 1 mm long solenoid coil with a self-inductance of 18 nH. The capacitor consists of an AlN substrate coated with a PdAu layer. The high-dielectric constant of AlN allows the use of a relatively small capacitor. The LC-circuit is coupled capacitively to a quarter lambda cable for fine-tuning and matching of the probehead to the spectrometer electronics (Fig. 2). The quality factor of the tuned probe, as measured with a HP5782C network analyzer, is $Q_{S11} = 13$ at a frequency of 400 MHz. Note that this Q_{S11} value is the quality factor of a matched circuit as used in the actual NMR experiments, various papers report the Q factor of a tuned but unmatched circuit which is two times the Q_{S11}.

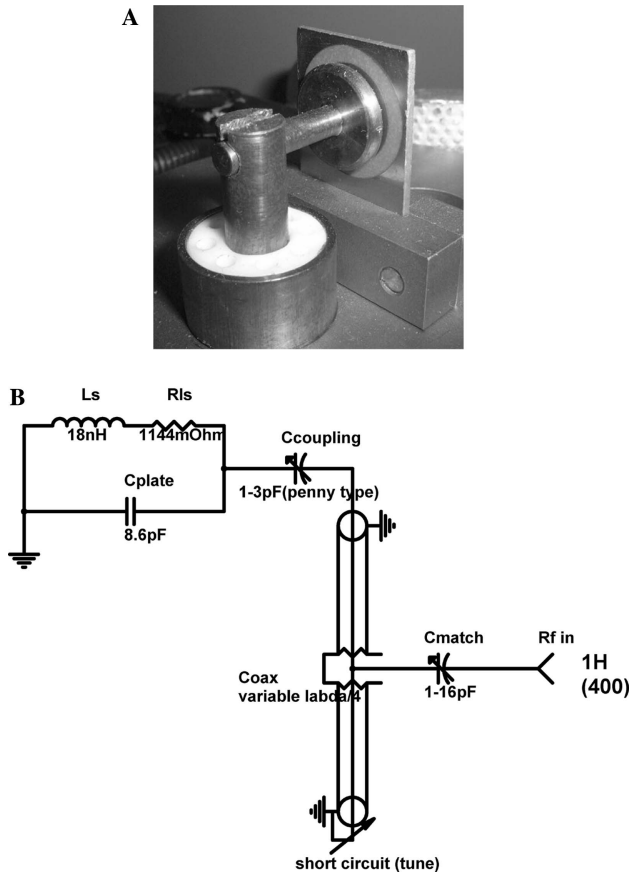

Fig. 2. (A) View of the assembled proton observation probehead looking at the coupling capacitor in front of the parallel resonance circuit. (B) Schematic circuit of the microcoil probehead for proton observation.

The narrowband X-nuclei probehead is of a similar design as the proton probe. The coil volume is the same but now the coil consists of 14 windings with a spacing of 70 μm resulting in a self-inductance of 30 nH. Again to reach the appropriate capacitance to tune the circuit with a relatively small capacitor a material with a high-dielectric constant and low dielectric losses was used ($MgO–CaO–TiO_2$ (IMPEX HighTech, Germany), $\varepsilon_r = 19.5$). This resonance circuit is put in parallel (by clamping) to a tuning capacitor whose value can be varied by about 5 pF by shifting a quartz plate between the capacitor plates. This allows tuning over a narrow bandwidth. The circuit is capacitively coupled via the matching capacitor to the rest of the circuit as shown in Fig. 3. Experimentally the quality factor of the probe was determined to be $Q_{S11} = 8.6$ at a frequency of 161.9 MHz.

As wide ranges of nuclei are potential candidates for microcoil analyses, a third probe was built allowing tuning over a broad frequency range. The microcoil used in this probehead has 16 turns made from round 60 μm insulated-copper wire. The core diameter of this wire is 45 μm. The wire is wound with a spacing of 60 μm on a polystyrene (Rexolite) tube with an inner-diameter of 200 μm (sample space) and an outer-diameter of 300 μm. The length of the coil is about 1000 μm. The coil is fixed with cyano-acrylate glue and covered with a

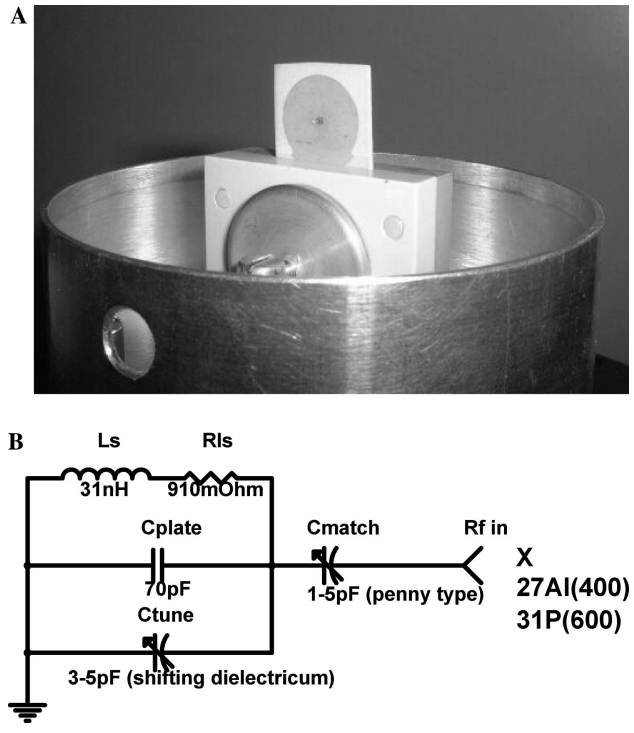

Fig. 3. (A) View of the assembled narrowband X-nuclei probehead with the parallel resonance circuit, with the coil in the center, protruding from the matching capacitor. (B) Schematic diagram of the circuit of the X-nuclei microcoil probehead.

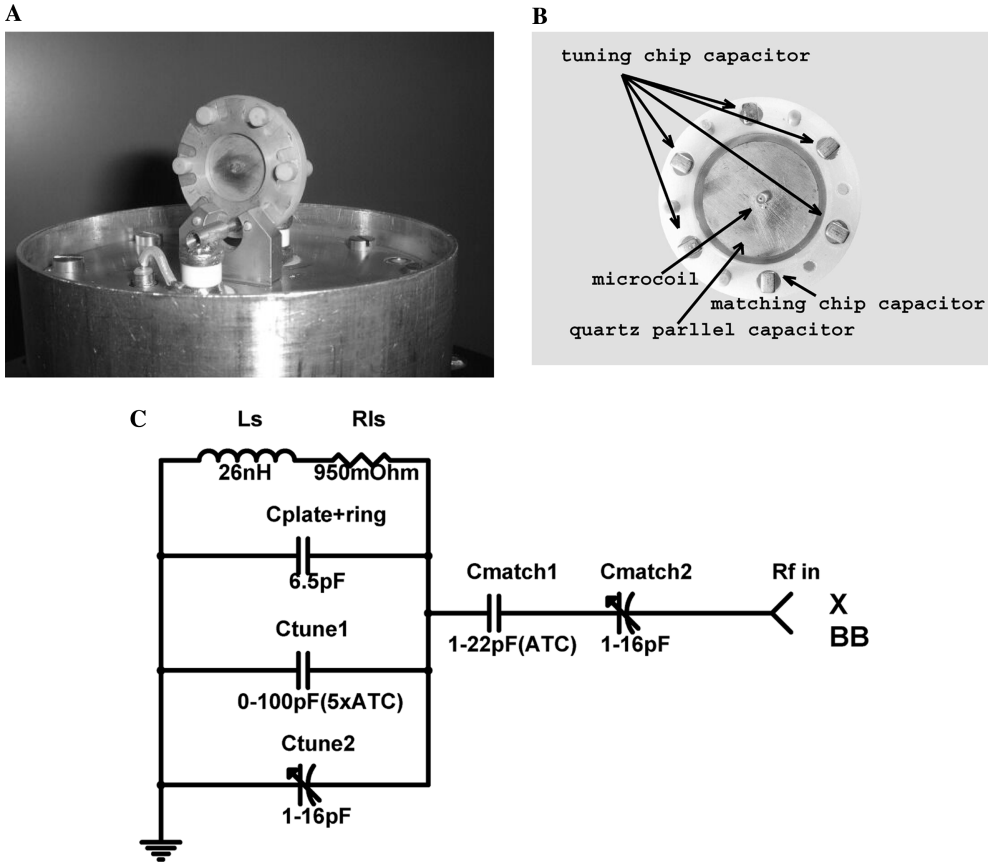

Fig. 4. (A) View of the assembled broadband X-nuclei probehead. (B) Parallel resonance circuit including coil, main tuning capacitor (Au coated quartz), five exchangeable chip capacitors, and one exchangeable matching capacitor. (C) Schematic drawing of the broadband probehead circuit.

KEL-F sleeve. The inductance of the coil is about 26 nH. The microcoil part is clamped into a plate capacitor and soldered to the capacitor contacts. The capacitor is made from a quartz plate of 1 mm thickness (dielectric) covered at two sides with a gold-plated (60 μm) copper foil. As quartz has a lower dielectric constant ($\varepsilon_r = 3.8$), compared to the previously used dielectrics, extra capacitors are needed for tuning the circuit. These are put in parallel to the main capacitor by clamping five fixed and one variable capacitor circularly between the plates of the main capacitor as is shown in Fig. 4. One side of the resonant circuit is directly connected to ground and the other side is connected to a matching capacitor. The matching capacitor consists of one variable capacitor and one fixed ceramic capacitor in series. After tuning and matching the circuit to 156.3 MHz (corresponding to the ^{27}Al frequency at 14.1 T), a quality factor Q_{S11} of 13.9 is obtained.

3. Probehead performance

The sensitivity of the probeheads is determined using a number of model samples. The experimental S/N is determined using a single-pulse excitation experiment; a free induction decay (FID) is acquired after a 90°-pulse excitation. In order to eliminate linewidth effects, the S/N is determined from the time domain data. In principle the $t = 0$ point of the FID holds all information about the line intensity independent of the linewidth. Due to the receiver dead time this point cannot be directly determined, however. Therefore we sampled the data at the highest speed (0.2 μs) the spectrometer allowed (but with different filter width) and performed linear back prediction, using the routine implemented in the Varian/Chemagnetics Spinsight software [19] to extrapolate the signal intensity at $t = 0$. The noise was determined as the rms noise in the acquisition channel after the signal had completely decayed. The number of spin in the sample was determined by carefully weighing the samples on a Sartorius S4 microbalance with 0.2 μg accuracy. From the experimental S/N at the given bandwidth and the spin density of the sample the number of spins is calculated that is needed to obtain a S/N of $1/\sqrt{\text{Hz}}$ in a single scan.

To get an impression about the sensitivity performance of the probeheads, theoretical sensitivities were calculated on the basis of Eq. (1). In principle all numbers in this equation are either constants or can be obtained experimentally fairly straightforward, except for

the specific coil parameters B_1/i and R_{noise}. Although B_1/i can be estimated from B_1 measurements as a function of applied RF-power and knowledge of the circuits' quality factor, the accuracy of such estimates is rather poor. We decided to simulate the coil parameters using finite element methods as implemented in the FEMM package [20]. The coil is modeled with its proper dimensions taking physical and electromagnetic (conductivity and permeability) properties of the wire material, circuit current, RF frequency, and B_0-field into account. Calculations were performed over a triangulated mesh of over 10,000 mesh points. The noise factor of the spectrometer system F was determined using the procedure as supplied by the spectrometer manufacturer [21] with the aid of a calibrated noise source (Hewlett Packard 346A-001). The noise factors of the systems at the frequencies used in the present study are summarized in Table 1.

Proton observations with the dedicated ^{1}H probehead operating at 400 MHz were performed on a 55.4 μg poly(dimethylsiloxane) sample, containing 3.9×10^{-6} mol of protons giving rise to a single-methyl resonance. A (time domain) S/N of 135.6 was obtained in a single scan with 130 kHz filter width. This translates into the necessity to have 4.8×10^{13} spins/$\sqrt{\text{Hz}}$ to obtain a $S/N = 1$ in a single scan. Although this is not the ultimate limit of detection, it is a convenient parameter to express the systems sensitivity. The actual limit of detection will furthermore depend on the type of experiment, the desired bandwidth for the spectrum and the time one can signal average, etc. The FEMM simulations predict a $S/N = 171.4$ for the given sample, or 3.7×10^{13} spins/$\sqrt{\text{Hz}}$ to get $S/N = 1$ in a single scan. Comparison of the experimental and simulated results show that these are in relatively good agreement. This means that the S/N in our circuit is mainly determined by the coil characteristics, as only the resistive losses are taken into account in the simulation. Considering the fact that, besides the coil, no other factors such as lead losses, etc. are included, we can conclude that the design of the RF-circuitry is rather efficient and does not induce major S/N losses. Similar numbers for the performance of microcoil circuits were recently reported by Minard and Wind [22].

In high-resolution NMR line broadening due to susceptibility effects is a problem using microcoils. The full width at half maximum (FWHM) of the PDMS resonance increased from 300 Hz in a conventional solid-state NMR probehead to 870 Hz in the microcoil probehead. Although this is a substantial line broadening it does not pose serious problems for wide-line applications. A line broadening of over 1 ppm is detrimental for possible high-resolution studies, however. As the sample volume is already restricted using the cylindrical vespel holder we think susceptibility effects are not the major line-broadening source. It turns out that the AlN substrate contains a Ni layer to improve adherence to the PdAu conductor. It may well be that this ferromagnetic nickel causes the observed line broadening.

Table 1
Noise figures form the spectrometers used in this study

Nucleus	Noise factor at probe port of infinity 400 (dB)	Noise factor at probe port of infinity 600 (dB)
^{1}H	2.80	2.25
^{31}P	2.41	1.96
^{27}Al	1.59	1.69

The noise factors were determined by replacing the probe by a calibrated noise source (Hewlett Packard; model No. 346 A-001).

Besides the sensitivity of the circuit we studied the B_1-field as a function of input power. Because of the reciprocity theorem very high RF-fields are expected at limited powers. Indeed using a power of only 5 W, an RF-field strength of 600 kHz is obtained. As the circuit is capable of handling high powers, a 4.7 MHz RF-field was obtained at an RF-power of 270 W (Fig. 5).

The availability of high-RF-fields facilitates many NMR experiments. In the first place excitation of very broad lines becomes a trivial task using either single-pulse excitation or Hahn echoes to overcome dead time effects. One can also think of very efficient homonuclear decoupling and/or two-photon excitation as was recently proposed by Michal [23]. As this is a second-order effect the effective field scales with B_1^2/B_0, so a 5 MHz RF-field at 400 MHz results in an effective field of 62.5 kHz which should allow efficient excitation and decoupling. Investigations to implement such schemes are in progress.

It should be noted that the RF-efficiency of small coils is not only interesting for solid-state NMR applications. Also for high-resolution studies at high fields efficient bandwidth coverage using low power is an important advantage as was pointed out by Li et al. [24] in their description of three- and four-frequency NMR probes for the study of small amounts of protein.

We monitored the RF-homogeneity of the coil by performing a nutation spectrum using a sample that is approximately 500 μm long, i.e., with the coil half filled. The nutation spectrum in Fig. 5 shows the RF-field distribution experienced by the sample. We see that the RF-field drops off from 4.7 MHz (the RF-field in the center of the coil), to about 3.8 MHz. This is roughly in accord with Eq. (2) from which one expects the on-axis RF-field to drop by 12.5% half way down the coil for an idealized coil. Fig. 5B also shows the calculated RF-field profile as obtained from the FEMM simulation; the RF-field from 20 μm^3 voxels in the coil center (500 μm × 250 μm × 250 μm) are scored over a frequency grid. The experimental RF-inhomogeneity is slightly larger than the calculated one. This is attributed to irregularities in the sample geometry, which is difficult to control and/or small irregularities in the coil winding. It should be

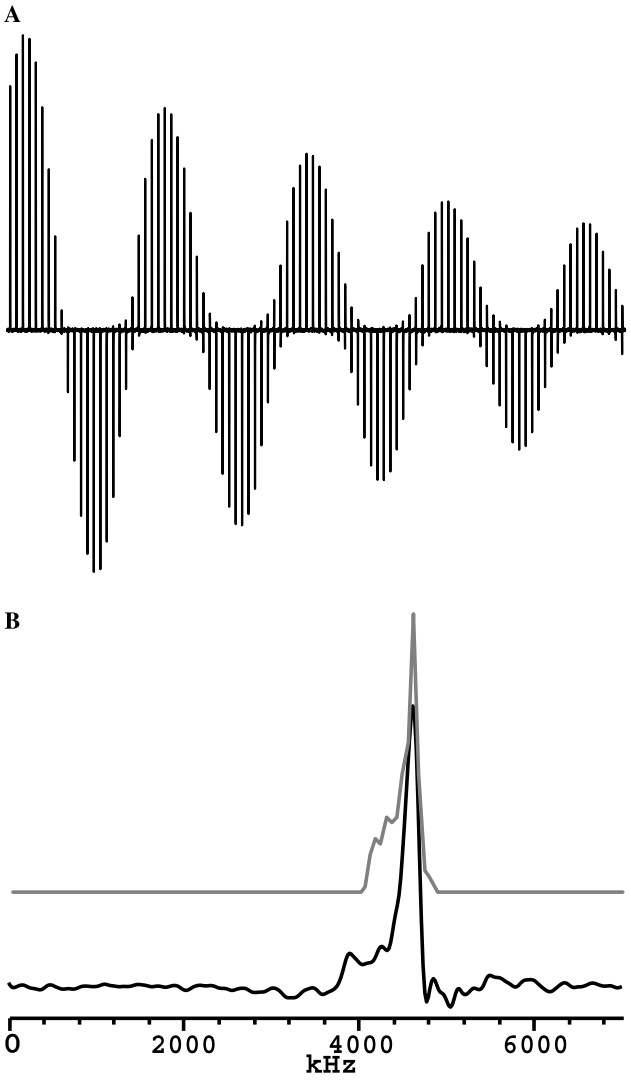

Fig. 5. (A) Nutation experiment on a sample of 500 μm × 250 μm × 250 μm Poly(dimethylsiloxane) placed at the center of the proton observation probehead. The pulse length was incremented from 0.05 to 1.00 μs in 0.01 μs steps. Thirty-two experiments were accumulated with 3 s recycle delay. The employed RF-power was 270 W resulting in an RF-field of 4.7 MHz. (B) Experimental RF profile (black line) and reconstructed RF profile from FEMM simulations (gray line) over a volume of 500 μm × 250 μm × 250 μm sample.

noted, however, that the relative homogeneity is better than that of a commercial static 5 mm probe. Finally, the signals for the shortest pulse lengths show no significant deviations. Their rectangular shape is well maintained, for a 150 ns pulse we observed a rise time of 30 ns and a decay time of 20 ns.

The narrowband X-nuclei probehead can be tuned around 160 MHz. It was used to observe phosphorus at 9.4 T (^{31}P, 161.9 MHz) and aluminum at 14.1 T (^{27}Al, 156.3 MHz). For ^{31}P the S/N evaluation was performed by single-pulse excitation of potassium dihydrogenphosphate (KH_2PO_4). The S/N was 11.4 after 64 scans for a sample weighing 67.6 μg using a filter width of 260 kHz. This means we need 4.0×10^{14} ^{31}P spins/$\sqrt{\text{Hz}}$ to get a $S/N = 1$ in a single scan. The calculated value, again taking only the RF-coil into account, amounts to 2.8×10^{14} spins/$\sqrt{\text{Hz}}$. So also for this probehead the losses are concentrated in the RF-coil. An effect on the resolution by the probehead was checked using a 1 M NaH_2PO_4 solution in water. The FWHM is 100 Hz, which is similar to the linewidth in a conventional solid-state NMR probehead, showing that susceptibility broadening is only minor for the chosen sample size and geometry. This observation gives support to our assumption that the line broadening observed in the proton probe is due to the presence of ferromagnetic material in the capacitor dielectric. For the present probe a different dielectric was chosen that does not have this problem. Finally, the RF-efficiency was tested using 4 W RF-power giving rise to a B_1-field of 310 kHz.

^{27}Al observation at 14.1 T operating at 156.3 MHz can be achieved by retuning the probehead without further changes to the circuit. A 140 μg single crystal of sapphire (α-Al_2O_3) was used as a test sample. Using a spectral width of 1.3 MHz a $S/N = 51.9$ is obtained after 16 scans for this sample containing 1.6×10^{18} aluminum spins. So 1.1×10^{14} ^{27}Al spins/$\sqrt{\text{Hz}}$ are necessary to get a S/N of 1 in one scan for this probehead in accord with the theoretical calculations (8.0×10^{13} spins/$\sqrt{\text{Hz}}$). An RF-field strength of 350 kHz, 1.3 MHz and 1.9 MHz is obtained at 5, 200, and 380 W, respectively.

The broadband probehead is tunable up to 300 MHz by exchanging capacitors, meaning coverage of all X-nuclei at 14.1 T. By adding an extra inductance parallel to the receiver coil it is even possible to tune the probehead to the proton frequency of 600 MHz at 14.1 T. The performance of this probehead is evaluated for ^{1}H and ^{27}Al. ^{27}Al observation of a 30.4 μg sapphire crystal (3.6×10^{17} aluminum atoms) gave a $S/N = 19.0$ after 256 scans at a 2 MHz receiver bandwidth, i.e., 2.1×10^{14} spins/$\sqrt{\text{Hz}}$ will give $S/N = 1$ in a single scan. This shows a rather large discrepancy with the calculated value of 7.0×10^{13} spins/$\sqrt{\text{Hz}}$ based on FEMM simulations. As the coil diameter was reduced an increase in sensitivity was expected compared to the narrowband probehead. Apparently, the added path length and the capacitors introduced to achieve the broadbandedness of this circuit are introducing serious losses to the circuit. Furthermore we suspect that the material of the coil holder and the employed glue to fix the coil induce significant dielectric losses. Further investigations are necessary to pinpoint the major source causing the sensitivity loss in this circuit. The resolution is checked with a 1 M $Al(NO_3)_3$ solution giving a linewidth of 46 Hz which means an insignificant broadening for any solid-state NMR application. Finally, a 260 kHz RF-field is obtained with 5 W RF-power. At powers of, respectively, 200 and 820 W, we get RF-fields of 1.7 and 3 MHz.

Table 2
RF-field strength achieved at different power levels and experimental and calculated sensitivity for the different probeheads using various model compounds

	^{1}H probe ∅ 400 μm	Narrowband X-nuclei ∅ 400 μm		Broadband ∅ 300 μm	
Nucleus	^{1}H @ 9.4 T	^{31}P @ 9.4 T	^{27}Al @ 14.1 T	^{27}Al @ 14.1 T	^{1}H @ 14.1 T
Frequency	400 MHz	161.9 MHz	156.3 MHz	156.3 MHz	600 MHz
RF-field	4.7 MHz	310 kHz	1.9 MHz	3 MHz	300 kHz
Power	270 W	4 W	380 W	850 W	5 W
Experimental sensitivity[a]	4.8×10^{13}	4.0×10^{14}	1.1×10^{14}	2.1×10^{14}	4.6×10^{14}
Theoretical sensitivity[a]	3.7×10^{13}	2.8×10^{14}	8.0×10^{13}[b]	7.0×10^{13}[b]	2.2×10^{13}

[a] Number of spins/$\sqrt{\text{Hz}}$ to get $S/N = 1$ in one scan.
[b] Adding up the intensity of all single-quantum transitions.

By adding a two-turn coil to the circuit the probe is tuned to 600 MHz for ^{1}H observation at 14.1 T. For 7.3 μg poly(dimethylsiloxane) (3.0×10^{17} spins) a S/N of 36.9 is obtained with 2048 scans at 650 kHz bandwidth, translating to 4.6×10^{14} spins/$\sqrt{\text{Hz}}$ for an $S/N = 1$ in one scan. This is an order of a magnitude worse than the theoretical 2.2×10^{13} spins/$\sqrt{\text{Hz}}$. As already discussed for the ^{27}Al observation significant losses are present in this circuit, which need further investigation. Inevitably the performance deteriorates further by adding a parasitic inductance.

The results obtained for the three probeheads are summarized in Table 2. The number of spins per hertz to get a $S/N = 1$ for one scan is order of 10^{14} for these coils with a diameter of several hundred micrometers. This shows that microcoils can be successfully implemented in solid-state NMR of mass-limited samples. The actual limit of detection will depend on the exact experiment, desired bandwidth, and the amount of signal averaging that can be applied. A remarkable feature of the circuits is that they can withstand high-power levels for such small structures. This can be used to generate exceptionally high RF-fields well in excess of a megahertz for most nuclei. This opens the way to new experiments and makes direct excitation of large bandwidths very easy. This is especially valuable for quadrupolar nuclei experiencing large quadrupolar interactions as will be demonstrated in the following section.

4. ^{27}Al microcoil NMR of minerals

To demonstrate the convenience of having large RF-fields at ones disposal we studied a single crystal and powdered sapphire sample and did a limited rotational study of a kyanite crystallite. For quadrupolar nuclei in natural and synthetic samples one is often faced with the problem that resonance frequencies are dispersed over several megahertz due to the quadrupolar interaction. Furthermore it can be a problem to obtain crystals of sufficient size to undertake a single-crystal study of a material. Application of microcoils alleviates both problems.

As described above ^{27}Al NMR signals of a 30.4 μg single crystal of sapphire were observed at 14.1 T in a 300 μm diameter microcoil. Sapphire has a single-Al site with a quadrupole coupling constant of 2.4 MHz and $\eta = 0$ [25]. Fig. 6A displays the spectrum of the single crystal obtained with a 150 ns pulse using an RF-field of 1.7 MHz. All five single-quantum transitions ($5/2 \leftrightarrow 3/2$, $3/2 \leftrightarrow 1/2$, $1/2 \leftrightarrow -1/2$, $-1/2 \leftrightarrow -3/2$, $-3/2 \leftrightarrow -5/2$) are clearly visible in the spectrum displaying a quadrupolar splitting of 80 kHz. Because of the even excitation of the various lines, they are observed with intensities very close to the theoretical ratios for a non-selective excitation of a spin 5/2 system (5:8:9:8:5). Using lower RF-fields the intensities of the satellite transitions are often diminished because they are less efficiently excited. This is a particular problem for powder spectra were the intensity in the satellites is dispersed over a large frequency range and are often hardly observed with respect to the narrow central transition which is only broadened by the quadrupolar interaction in second-order. Fig. 6B shows the experimental and theoretical ^{27}Al spectrum of powdered sapphire using a two-pulse echo. The powder lines of the satellite transitions are spread out over 720 kHz but are clearly observed without significant distortions, reflecting the features of a site with $C_{\text{qcc}} = 2.4$ MHz and $\eta = 0$ in accord with the literature data [24].

The natural mineral kyanite (Al_2SiO_5) has four crystallographically different sites with NMR parameters summarized in Table 3 [26]. As the quadrupolar coupling constant of the sites in this mineral goes up to 10 MHz one can expect resonances dispersed over a bandwidth of several megahertz. A single-crystal NMR study was performed in the narrowband X-nuclei probe using an RF-field of 1.7 MHz. Fig. 7 displays single-crystal spectra with a rotation of ~20° about an arbitrary axis. The single-quantum transitions of all four sites are visible dispersed over a spectral width of up to 4 MHz. Besides the kyanite resonances we observe the sapphire signals originating from this material used in the probe construction. This shows the use of microcoils for obtaining accurate NMR parameters from small single crystals. A systematic single-crystal study

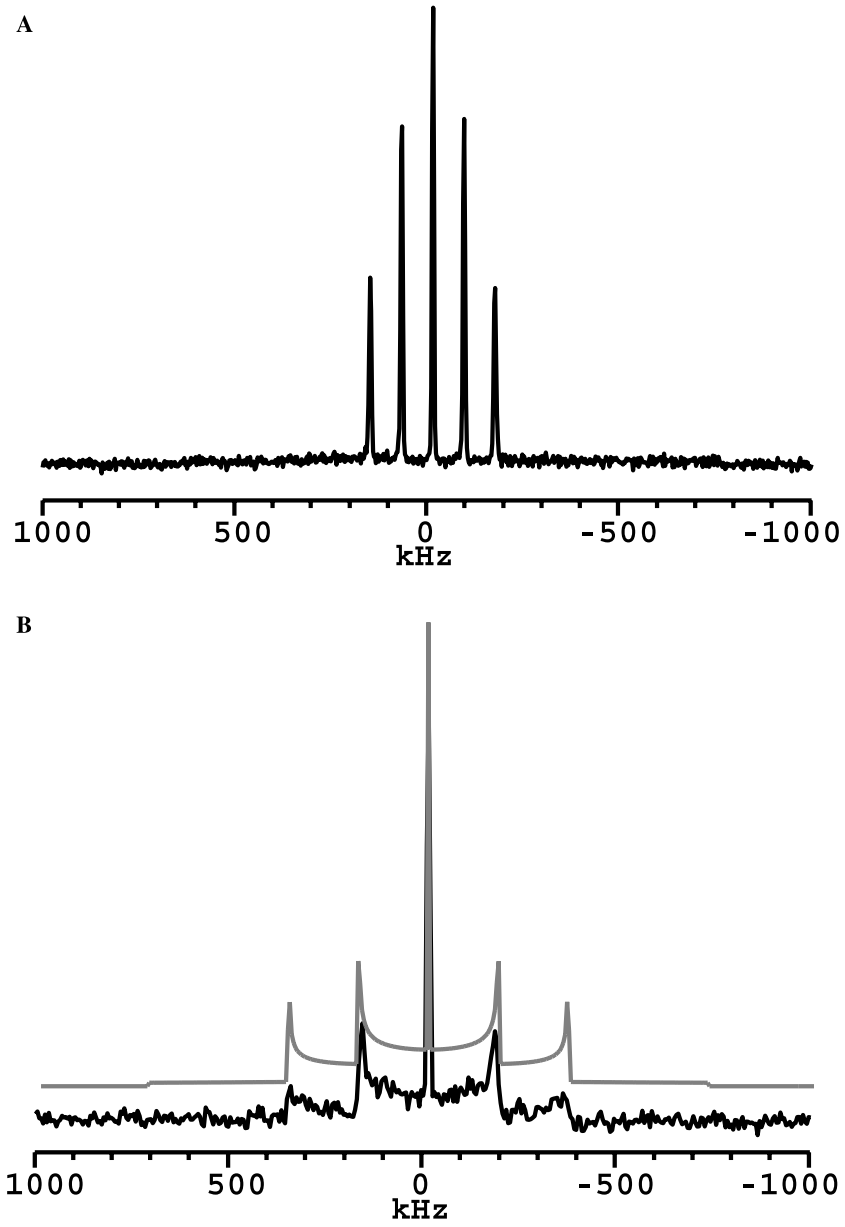

Fig. 6. (A) ^{27}Al spectrum of a sapphire single crystal obtained with the broadband microcoil probehead at 14.1 T. This spectrum is obtained by single-pulse experiment averaging 1024 scans. A 60 sec pulse delay was used. The experimental ratio of single-quantum peak-integrals 5.0:7.8:9.0:7.6:4.7 is very close to the theoretical 5:8:9:8:5. (B) ^{27}Al spectrum of powdered sapphire obtained in the same probehead (black line). A Hahn echo pulse sequence is averaging over 4096 accumulations using a 60 s pulse delay. The powder lineshape of the satellite transitions agree with theoretically calculated spectrum (gray line) from literature data ($C_{qcc} = 2.4$ MHz, $\eta = 0$) [24].

Table 3
^{27}Al NMR parameters of kyanite (Alemany et al. [25])

	Site 1	Site 2	Site 3	Site 4
C_{qcc} (MHz)	10.1	3.8	6.4	9.2
η	0.27	0.85	0.70	0.38
δ_{CS} (ppm)	13.0	4.0	5.7	5.9

demands the construction of a micro unit allowing accurate rotation of the crystal around two independent axes.

5. Conclusion

With the ongoing miniaturization of analytical methods, there lies a great challenge for an intrinsically insensitive technique such as NMR. It is therefore that we witness a renaissance of technique development in magnetic resonance striving to improve the sensitivity. For example there is a renewed interest in dynamic nuclear polarization, the use of optically polarized gasses, increasingly higher field strength using Bitter magnets and even pulsed magnets and mechanical detection

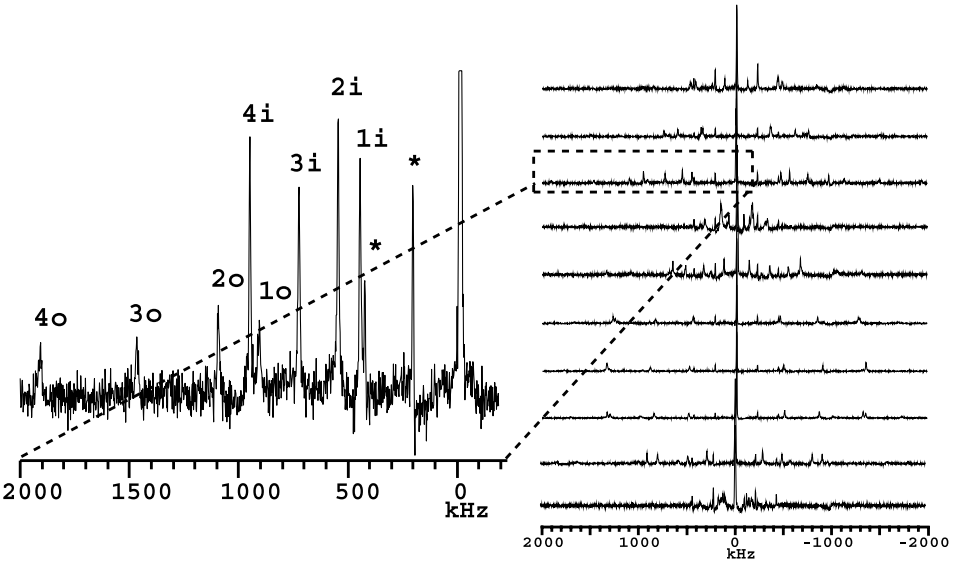

Fig. 7. ^{27}Al NMR spectra of a kyanite single crystal (500 μm × 200 μm × 200 μm). The crystal is rotated over 20° about an arbitrary spectrum. As shown in the expanded view, all satellite transition for the four different sites are observed (i inner transitions, o outer transition). * indicate sapphire satellite transitions from the probe material. The spectra are obtained with the narrowband X-nuclei microcoil probehead using single-pulse excitation averaging 64k acquisitions with a 0.25 s pulse delay.

of magnetic resonance. The development of NMR probes based on miniaturized coils has also attracted a lot of attention over the last decade, especially for high-resolution NMR of small volumes of liquid samples and high-spatial resolution imaging of biological samples. The advantage of the microcoil approach over the previously mentioned techniques is that it allows the use of all conventional NMR techniques without adaptation. A further advantage is the possibility to implement NMR experiments in intrinsically less homogeneous external fields such as resistive high-field magnets or "inside–out" magnets as used in the NMR-mouse. Finally, large variations of environment parameters such as pressure and temperature should be less demanding when realized in a micro setup.

Although MAS rotors have gotten smaller and smaller, the application of microcoils in solid-state NMR has been somewhat neglected. In the present contribution it is shown that microcoils hold great promise in this field. Microcoil probeheads with coil diameters of 300 and 400 μm were built and tested. It is demonstrated that the sensitivity per unit volume is increased, allowing the observation of 10^{13}–10^{14} spins in a reasonable amount of time. The results show that the circuits should be carefully designed and optimized at the observed frequency. A broadband solution did not perform as well. A major benefit is the enormous RF-fields that can be generated with these probes. At RF-powers of only a few Watts RF-fields of hundreds of kilohertz are generated, which allow easy operation of many NMR experiments. With RF-powers of several hundred Watts, RF-fields reach up into the megahertz regime. This will make many conventional NMR experiments much easier to perform, e.g., efficiently decouple or excite spins over a large bandwidth. Especially experiments based on "higher-order" effects such as the excitation and conversion of multiple-quantum transitions, two-photon absorption and overtone NMR should benefit greatly from these high RF-fields.

Acknowledgments

The authors would like to thank Mr. J. van Os and Mr. G. Janssen and Dr. J. van Bentum for their support and advise. Mr. B. van den Berg is acknowledged for his craftmenship in micromachining the microcoil parts. This work is part of the research programme of the Stichting voor Fundamenteel Onderzoek der Materie (FOM, financially supported by the Nederlandse Organisatie voor Wetenschappelijk Onderzoek (NWO)) and Philips Research. We thank Dr. J. Jansen, Dr. P. van Tilborg, and Dr. J. Pikkemaat (Philips CFT, Materials Analysis) for stimulating discussions.

References

[1] D.I. Hoult, R.E. Richards, The signal-to-noise ratio of the nuclear magnetic resonance experiment, J. Magn. Reson. 24 (1976) 71–85.
[2] D.L. Olson, T.L. Peck, A.G. Webb, R.L. Magin, J.V. Sweedler, High-resolution microcoil ^{1}H-NMR for mass-limited, nanoliter-volume samples, Science 270 (1995) 1967–1970.
[3] A.G. Webb, S.C. Grant, Signal-to-noise and magnetic susceptibility trade-offs in solenoidal microcoils for NMR, J. Magn. Reson. B 113 (1996) 83–87.

[4] A.G. Webb, Radiofrequency microcoils in magnetic resonance, Prog. Nucl. Magn. Reson. Spectrosc. 31 (1997) 1–42.
[5] R. Subramanian, W.P. Kelley, P.D. Floyd, Z.J. Tan, A.G. Webb, J.V. Sweedler, A microcoil NMR probe for coupling microscale HPLC with on-line NMR spectroscopy, Anal. Chem. 71 (1999) 5335–5339.
[6] J.D. Trumbull, I.K. Glasgow, D.J. Beebe, R.L. Magin, Integrating microfabricated fluidic systems and NMR spectroscopy, IEEE Trans. Biomed. Eng. 47 (2000) 3–7.
[7] C. Massin, A. Daridon, F. Vincent, G. Boero, P.A. Besse, E. Verpoorte, N.F. de Rooij, R.S. Popovic, A Microfabricated probe with integrated coils and channels for on-chip NMR spectroscopy, in: J.M. Ramsey (Ed.), Micro Total Analysis Systems, 2001, pp. 438–440.
[8] T.L. Peck, R.L. Magin, P.C. Lauterbur, Design and analysis of microcoils for NMR microscopy, J. Magn. Reson. B 108 (1995) 114–124.
[9] R.A. Wind, K.R. Minard, G.R. Holtom, P.D. Majors, E.J. Ackerman, S.D. Colson, D.G. Cory, D.S. Daly, P.D. Ellis, N.F. Metting, C.I. Parkinson, J.M. Price, X.W. Tang, An integrated confocal and magnetic resonance microscope for cellular research, J. Magn. Reson. 147 (2000) 371–377.
[10] P. Glover, P. Mansfield, Limits to magnetic resonance microscopy, Rep. Prog. Phys. 65 (2002) 1489–1511.
[11] L. Ciobanu, A.G. Webb, C.H. Pennington, Magnetic resonance imaging of biological cells, Prog. Nucl. Magn. Reson. Spectrosc. 42 (2003) 69–93.
[12] Z. Gan, P. Gor'kov, D. Massiot, L. Butler, A. Samoson, Solid state NMR of quadrupolar nuclei at very high fields, Ann. Res. Rev. NHMFL (2001) 217.
[13] M. Horvatic, C. Berthier, High field NMR in strongly correlated low-dimensional fermionic systems, Int. J. Mod. Phys. B 16 (2002) 3265–3270.
[14] P.J.M. van Bentum, J.C. Maan, J.W.M. van Os, A.P.M. Kentgens, Strategies for solid-state NMR in high-field Bitter and hybrid magnets, Chem. Phys. Lett. 376 (2003) 338–345.
[15] B. Blumich, P. Blumler, G. Eidmann, A. Guthausen, R. Haken, U. Schmitz, K. Saito, G. Zimmer, The NMR-mouse: construction, excitation, and applications, Magn. Reson. Imaging 16 (1998) 479–484.
[16] K.R. Minard, R.A. Wind, Solenoidal microcoil design. Part I: optimizing RF homogeneity and coil dimensions, Concepts Magn. Reson. 13 (2001) 128–142.
[17] K.R. Minard, R.A. Wind, Solenoidal microcoil design—part II: optimizing winding parameters for maximum signal-to-noise performance, Concepts Magn. Reson. 13 (2001) 190–210.
[18] D.I. Hoult, Sensitivity of NMR experiments, in: D.M. Grant, R.K. Harris (Eds.), Encyclopedia of Nuclear Magnetic Resonance, 1996, pp. 4256–4266.
[19] Varian/Chemagnetics, NMR acqusition and process software spinsight version 4.3.2, 2003.
[20] D. Meeker, Finite Element Method Magnetics (FEMM), 2003. Available from <http://femm.berlios.de/>.
[21] Varian/Chemagnetics, Console electronic tests to verify console performance relating to NMR S/N, 1999. Available from <ftp://ftp.nmr.varianinc.com/chemagnetics/>.
[22] K.R. Minard, R.A. Wind, Picoliter H-1 NMR spectroscopy, J. Magn. Reson. 154 (2002) 336–343.
[23] C.A. Michal, Nuclear magnetic resonance noise spectroscopy using two-photon excitation, J. Chem. Phys. 118 (2003) 3451–3454.
[24] Y. Li, T.M. Logan, A.S. Edison, A. Webb, Design of small volume HX and triple-resonance probes for improved limits of detection in protein NMR experiments, J. Magn. Reson. 164 (2003) 128–135.
[25] T. Vosegaard, H.J. Jakobsen, Al-27 chemical shielding anisotropy, J. Magn. Reson. 128 (1997) 135–137.
[26] L.B. Alemany, S. Steuernagel, J.P. Amoureux, R.L. Callender, A.R. Barron, Very fast MAS and MQMAS NMR studies of the spectroscopically challenging minerals kyanite and andalusite on 400, 500, and 800 MHz spectrometers, Solid State Nucl. Magn. Reson. 14 (1999) 1–18.